Arabian Journal of Geosciences (2021) 14: 2341
https://doi.org/10.1007/s12517-021-08679-8

ORIGINAL PAPER

Assessment of water recharge source of geothermal systems in Garhwal Himalaya (India)

Akshaya Verma[1] · Sameer K. Tiwari[1] · Amit Kumar[1] · Kalachand Sain[1] · Santosh K. Rai[1] · Sunita Kumari[1]

Received: 7 June 2021 / Accepted: 17 October 2021 / Published online: 4 November 2021

Abstract

The geothermal systems in the Himalaya are complex, and their genesis, circulation pattern and processes of sustenance are largely unknown. The present study aims to systematically analyse the characteristics of oxygen and hydrogen isotopes, major ion data and strontium ratio ($^{87}Sr/^{86}Sr$) of geothermal systems, river waters and rainwater to understand the movement of groundwater and the mechanisms for the formation of geothermal systems in the region. Further, the strontium isotope was also used to understand the fluid source of geothermal systems. Field observations show that the geothermal waters have a higher temperature, hydraulic pressure and elevated δD and $\delta^{18}O$ values than river waters. Thus, large river systems are not the principal recharge source of geothermal systems. Meteoric water (rain and snowmelt) in high mountains can infiltrate and circulate deep down the active tectonic belts or sutures and recharge geothermal systems. The cold surface water evolves into high-temperature thermal water after deep circulation and is discharged as a geothermal spring at the surface, under a high water-head difference. Therefore, the large-scale geothermal systems in the Garhwal Himalaya develop and are maintained by rapid groundwater circulation and interaction with a heat source. Further, the water temperatures of these systems in Garhwal Himalaya have remained the same over the period 1975–1994 (Geological Survey of India) and 2010–2016 (this study) with an error of < 5%.

Keywords Geothermal systems · Groundwater · Isotopes · Himalaya

Introduction

The Himalayan range is an active mountain chain that hosts many geothermal systems in natural and artesian conditions that eject hot waters and volatiles with varied temperatures and chemical compositions. The Himalaya-Karakoram region stretching from Pamir to Yunnan has documented ~ 600 geothermal systems (Gyanprakash and Raina 1975; Tong and Zhang 1981). The South Asia region is under active tectonic process over the last 50 million years, producing the Himalayan orogeny by continent–continent collision. The underthrusting of the Indian plate beneath the Eurasian plate has led to the rise of the Himalaya through the process of crustal thickening (Molnar et al. 1987; Bilham et al. 1997; Hochstein and Regenauer 1998) and crustal melting (Searle et al. 1997; Henry et al. 1997). Steep geothermal gradients that can force hydrothermal circulations along with degassing of volatiles are associated with the rapid uplift and exhumation in such mountain belts (Koons and Craw 1991; Jenkin et al. 1994; Koons et al. 1998; Tiwari et al. 2020). Therefore, geothermal circulation can be an important phenomenon in the thermal budget of an orogeny (Ingebritsen et al. 2001; Forster and Smith 1989; Manga 1998; Derry et al. 2009). The world's rarest and distinct geothermal systems have developed in the deeply incised valleys beside the main boundary thrust (MBT), the main central thrust (MCT) and the Indus Tsangpo suture zone (ITSZ) with the upliftment of the Himalayan mountain chain (Evans 2003; Evans et al. 2004; Becker et al. 2008). The distribution of geothermal systems is asymmetric to the Himalayan axis. However, several of these systems in northwest Himalaya, especially those with surface temperatures of T_s ~ 90 °C, fall next to the main thrust zones, indicating that these have structural control (Hochstein and Regenauer 1998;

Responsible Editor: Broder J. Merkel

✉ Akshaya Verma
akshayaverma5@gmail.com

[1] Wadia Institute of Himalayan Geology, Dehra Dun, 33, GMS Road, Dehra Dun 248001, Uttarakhand, India

Newell et al. 2008; Evans et al. 2008; Rai et al. 2015; Tiwari et al. 2016b).

Geothermal systems are of cyclic and storage types globally. Himalayan geothermal systems fall in the cyclic category, where water is meteoric (Gupta and Roy 2006), percolates to deeper depths and then heats and upwells to the surface (Tiwari 2014). Some previous studies have focused on the formation of geothermal systems in the Himalayan region and assume that meteoric waters infiltrate and circulate within a restricted space where heat is transferred from a source to the sink to recharge the geothermal systems (Chandrajith et al. 2012; Tan et al. 2014; Tiwari et al. 2016a).

Based on geophysical exploration, it has been confirmed that the magmatic input through crustal remelting is the principal heat source in the Tibetan Plateau (Tan et al. 2014). The heat source for geothermal systems could be a low-temperature system, in which temperature increases with depth or a magmatic intrusion (> 600 °C) that has reached relatively shallow depths of 2 to 5 km (Harinarayana et al. 2006). The circulating fluid reservoir could extract heat from a volume of hot permeable rocks overlain by an impermeable layer. The geothermal fluid is water, which exists as a liquid or vapour phase depending on its temperature and pressure. This water often carries chemical constituents like boron (B), lithium (Li), caesium (Cs), rubidium (Rb), strontium (Sr), arsenic (As), iron (Fe) and uranium (U) (Gupta and Agarwal 2001; Evans et al. 2003; Tan et al. 2014) and gases such as CO_2, H_2S, SO_2, He and CH_4 (Cinti et al. 2009). Zones of geomagnetic anomalies, shallow earthquakes and gravity anomalies are generally associated with these non-eruptive systems (Tiwari et al. 2020) and other processes in these settings like heat flow and migration of magmatic fluids from the deep to the surface (Azeez and Harinarayana 2007; Veeraswamy et al. 2010; Rawat 2012). However, previous studies have discussed the heat source of geothermal systems based on geological and geophysical data. Only a few have used stable water isotopes to observe and characterise the relationship between the formation mechanism, heat source and geochemistry of geothermal waters (Chandrajith et al. 2012; Tan et al. 2014; Tiwari et al. 2016a).

Given the diverse stable water isotopic compositions of geothermal springs, cold springs, river water, rainfall, snowfall and glacial meltwater, it offers a tremendous opportunity to trace the groundwater circulation, including recharge, runoff and discharge (Clayton et al. 1966; Clark and Fritz 1997; Tan et al. 2012, 2014; Tiwari et al. 2016a). This work aims to scientifically analyse the characteristics of stable water (hydrogen and oxygen) and radiogenic strontium isotopes ($^{87}Sr/^{86}Sr$) in different components of the hydrological cycle (geothermal systems, cold springs, river water, rainfall, snowfall and glacial meltwater) and to understand the circulation and source of water, heat source and hydraulic gradients to maintain the geothermal systems in Garhwal Himalaya.

Study area

The Garhwal region of the central Himalaya receives both the Indian summer monsoon (ISM) and westerlies which influence the rivers and streams draining the area. The Ganga River system has two major proglacial rivers, i.e. Bhagirathi and Alaknanda, and spreads over an area of ~ 30,000 km^2. Major streams of the region forming the headwaters of the Ganga carry 70–80% of their annual flow during the summer monsoonal months (Bruijnzeel and Bremmer 1989). Most of the rainfall leaves the area as direct surface runoff, and a little percolates to augment the dissected groundwater aquifers (Choubey et al. 1999) that ultimately return to the surface in the form of springs.

Geological setup and geothermal activity

The Himalayan tectonic structure is a blend of complex processes that function on different time scales. It conglomerates the Himalayan orogen, active foreland basin and major depositional systems like the Indus and the Bengal fans. The northwest and northeast Himalayan syntaxes are the marked bands of strike on both ends of the Himalaya (Tiwari 2014). The orogen is differentiated by ITSZ in the north, the Chaman fault in the west, the Sagging fault in the east and the Main Frontal Thrust (MFT) in the south (LeFort 1975). South-north division of the Himalaya starts from the Shivaliks; proceeding to the Lesser, Higher and Tethys Himalaya; and finally the Indus Suture Zone, which connects with the Trans-Himalaya (Auden 1937). These geographical and geological zones continue along the entire Himalayan arc (Gansser 1964; LeFort 1975). Thus, Garhwal Himalaya provides a perfect site for learning the diverse geological processes related to mountain building. Many researchers in recent years have been motivated by the potential of the region to decipher the feedback procedures between lithospheric deformation and atmospheric circulation as a driver of global climate change (e.g. Molnar 1987; Harrison et al. 1992, 1998; Royden et al. 1997; Ramstein et al. 1997; Tapponnier et al. 2001; Beaumont et al. 2000; Yin et al. 2002). This study covers the geothermal systems of Garhwal Himalaya in Alaknanda, Bhagirathi and Yamuna valleys along the MCT zone (Heim and Gansser 1975).

The Higher Himalayan Crystalline (HHC) rocks along these river valleys, separate from the Tethyan Himalaya to the north by the South Tibetan Detachment (STD) and from the Lesser Himalaya to the south by the southern strand of the MCT (Munsiari Thrust, or MCT-I, Fig. 1). The HHC contains high-grade gneisses, metabasite, quartzite, schist and granite, with limited carbonate and calc-silicate rocks

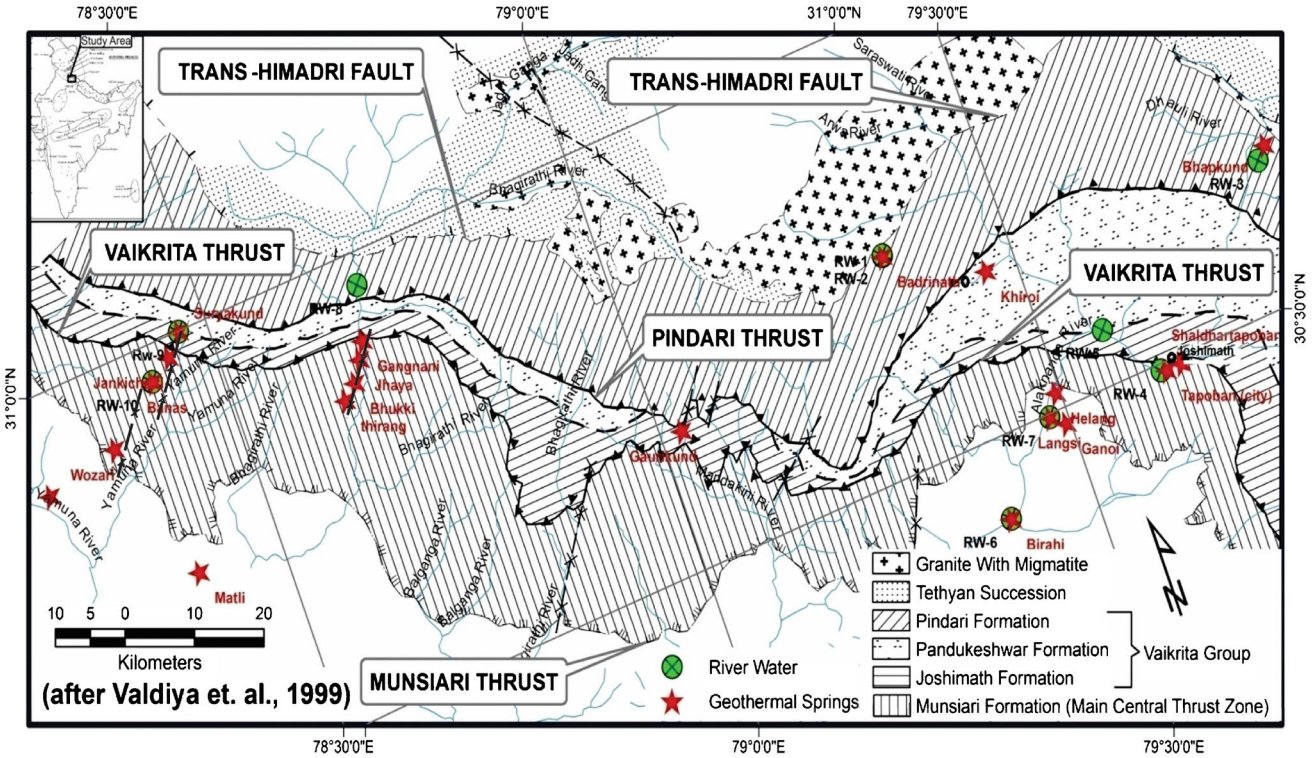

Fig. 1 Geological map of the Garhwal Himalaya with details of sampling locations of geothermal systems and river waters

(Aggarwal and Kumar 1973). The metamorphic grade of the HHC increases from biotite in the south with chlorite phyllite, chlorite schists and metabasic rock south of the MCT-I to kyanite and sillimanite bearing rocks north of the Vaikrita Thrust (or MCT-II; Sachan et al. 2001). It is the response of an inclined fault that got detached from the upper crust along a sub-horizontal zone at an inclination of 30° to 40° northward. It has also suffered a thrusting up to a depth of ~ 125 km which brought basement rocks up to the surface through ductile deformation (Roy and Valdiya 1988). Nearby the MCT in the Lesser Himalayan zone, the metamorphic and associated granite rocks are found severely deformed and compressed (Bhattacharya 1985). The majority of geothermal systems are around the MCT zone (flanked by MCT-I and MCT-II) in the Garhwal Himalaya, a region of high heat flow ($130 \pm 30 mW/m^2$) and high-temperature gradient ($60° \pm 20$ °C/km) that contrasts with the low heat flow ($41 \pm 10 mW/m^2$) and the low-temperature gradient ($17° \pm 5$ °C/km) of the lower Himalaya, south of the MBT (GSI 1991). Hence, sub-surface temperatures are high in the MCT zone, possibly due to the presence of partial melts and their associated fluids or perhaps simply due to coupled erosion-rock uplift (Derry et al. 2009). The electrical resistivity below 10Ω-m at 10–20-km depth in the MCT zone, along both the Bhagirathi and Alaknanda valleys, is thought to represent either partial melt or metamorphic fluids (Rawat et al. 2014) at moderate to high temperatures, thus providing a continuous heat source for the geothermal systems in the region.

The geothermal systems of Garhwal Himalaya largely fall in the central crystalline zone consisting of the Munsiari formation of the lower Himalayan crystalline sequence (LHCS) followed by the Vaikrita group of the greater Himalayan sequence (GHS) including Joshimath, Pandukeshwar and Badrinath formations. The Munsiari formation includes garnet-bearing mica schists, calc-silicate lenses and quartzite (Gururajan and Choudhuri 1999). The mineral assemblage within the Munsiari formation includes quartz, biotite, plagioclase, garnet, staurolite, muscovite, graphite and andalusite. The MCT in the Garhwal region is the ductile shear zone between the micaceous quartzites and chlorite-biotite schists of the Munsiari formation and the kyanite gneisses of the Joshimath formation. The Joshimath formation has a sequence of pelitic gneisses with schistose interlayers. It has a mineral assemblage of quartz, biotite, plagioclase, garnet, staurolite, muscovite, kyanite, chlorite, calcite, graphite, titanite and opaques (rutile, ilmenite). The Joshimath formation grades from metapelites to meta-arkose of Pandukeshwar formation. The Pandukeshwar formation consists of meta-arkose and quartzite. The meta-arkose is primarily medium- to fine-grained and is interlayered with kyanite-bearing schist (Paul 1998). Mineral assemblages in this formation include quartz, K-feldspar, plagioclase, muscovite, biotite, garnet, chlorite and opaques (rutile,

ilmenite, Cr-rich spinel). The Badrinath formation primarily consists of migmatitic metapelites and calc-silicates that grade upward from the meta-arkose of the Pandukeshwar formation. The Badrinath formation is bounded at the top by the STD and structurally overlain by the unmetamorphosed Martoli formation of the Tethyan Sedimentary Series. The metapelites of the Badrinath formation have a similar mineral assemblage to the Joshimath formation with the addition of sillimanite (quartz, biotite, plagioclase, garnet, staurolite, muscovite, kyanite, sillimanite, cordierite, chlorite, calcite, graphite, rutile and ilmenite) (Spencer et al. 2012). Calc-silicate layers generally contain calcite, diopside, quartz, hornblende, biotite, scapolite, actinolite and tremolite (Paul 1998; Spencer et al. 2012). Migmatitization of the Badrinath formation occurs ~ 16 km up the structural section from the MCT-II and increases upward to the STD. Migmatite stringers coalesce in the upper Badrinath formation where large leucogranite bodies intrude the surrounding metasediments. The leucogranite bodies consist of quartz, K-feldspar, plagioclase, muscovite, biotite, garnet, tourmaline, sericite (secondary) and chlorite (secondary).

Following the pioneering works of Auden (1937) and Heim and Gansser (1975), numerous geological studies have been carried out along the Yamuna, Bhagirathi, and Alaknanda valleys of the Garhwal Himalaya (Valdiya, (1980; 1981; 1988); Thakur and Rawat (1992)). Details of occurrences, discharge type and lithological formation of geothermal systems are given in Table S1.

Methodology

A total of twenty (20) samples of geothermal systems and ten (10) samples of river water associated with these geothermal systems were collected during 2010, 2012, 2013 and 2017 for the isotope (stable and radiogenic) and geochemical characteristics of the geothermal systems (Fig. 2A–F). Besides, glacier ice (01), snow (03), high-altitude rainfall (04) and meltwater (04) samples were also collected from Dokriani Glacier during 2010, 2013 and 2014. The snow-pit profile was conducted in May 2013 in the ablation zone of Dokriani Glacier (Fig. 2G). Geothermal spring water samples were collected close to their mouth, while river/glacial meltwaters were collected from the middle of the stream (Fig. 2H). The altitudinal range for all samples varies from 800 to 4068 m above sea level (asl). All water samples were filtered and stored in pre-cleaned HDPE amber colour bottles (Tarson®). One aliquot of the filtered water samples was poisoned by adding a 10 µL saturated solution of $HgCl_2$ (Sigma-Aldrich®) to prevent biological growth for stable isotope analyses. The physical parameters of all water samples were measured in situ (Fig. 2), including the temperature (°C), pH and electrical conductivity (µS/cm, EC) as per established methods (Dalai et al. 2002; Tiwari et al. 2016a, b) using the multi-electrode probes (The LaMotte pH 6 Series, Con6 meter) during the sampling with an average precision of ± 0.01 for conductivity, ± 0.05 for pH and ± 0.05 °C for temperature.

Chloride (Cl^-) and dissolved silica (SiO_2) analysis

Chloride (Cl^-) of the samples was analysed using ion chromatography (Dionex series ICS-5000) at the Wadia Institute of Himalayan Geology (WIHG) Dehradun. The calibration of the instrument and analysis of samples was done following the procedure of Tiwari et al. (2016a, b, 2020). The precision based on repeat analysis was ± 5% (1SD). Further, the dissolved silica was analysed in an un-acidified, filtered aliquot of the samples using a quadrupole inductively coupled plasma-mass spectrometer (ICP-MS) at WIHG (Tiwari 2014). The reproducibility of the measurement for dissolved silica was ± 5% (1SD).

Isotopic analysis ($\delta^{18}O$ ‰$_{vsmow}$, δD ‰$_{vsmow}$ and $^{87}Sr/^{86}Sr$ ratio)

The measurement of the stable oxygen isotope ($\delta^{18}O$) was carried out at the Isotope Ratio Mass Spectrometry Laboratory (IRMS) at WIHG following the established method by Tiwari et al. (2016a, b, 2018, 2020), Verma et al. (2018) and Kumar et al. (2018). The analytical procedure for the measurements of δD is almost similar to that of $\delta^{18}O$ except for the equilibration method where a platinum stick is placed into the vial before flush filling (Tiwari et al. 2016a, b; Verma et al. 2018; and Kumar et al. 2018). IRMS was calibrated with primary standards of GISP and VSMOW supplied by IAEA for measurements at regular intervals (Table S2, Craig 1961b). The reproducibility of measurement was 0.06‰ and 1‰ (1SD) for $\delta^{18}O$ and δD, respectively.

For Sr isotopic measurement of water samples, Sr specific resin (Eichrom) was used. The filtered water sample was loaded on the Sr specific resin in a clean chemistry lab. Milli-Q water was used to elute the pure Sr fraction. This fraction was dried and then made up using 3 N HNO_3 (Chatterjee and Singh 2012). Sr isotopic measurement of the samples was analysed using Multiple Collector ICP-MS (Neptune Plus, Thermo Fisher Scientific) in static mode. Instrumentation mass bias correction was done using the $^{88}Sr/^{86}Sr$ ratio (typical value: 8.375209 with exponential law). The isobaric interferences of Rb and Kr are corrected by measuring ^{85}Rb and ^{83}Kr using natural abundances. However, the signal of ^{85}Rb and ^{83}Kr was weak. A total of 40 cycles for each measurement were run with an integration time of about 8.3 s per cycle. The total measurement time was approximately 6 min for each run.

Fig. 2 Field photographs showing (**A**) Alaknanda at Badrinath, (**B**) release of the jet stream at Tapovan geothermal spring, (**C**) sampling at Vishnuprayag, (**D**) field measurements of physical parameters at Helang, (**E**) vent of geothermal system at Gangnani, (**F**) field measurements at Suryakund, Yamnotri, (**G**) snow pit sampling, and (**H**) temporary gauging site at Dokriani Glacier

Results and discussions

Details of all sample results are given in Table 1, whereas that of glacier melt/snow samples collected in different years and cold springs are shown in Tables 2 and S3. The pH of geothermal systems varied from 5.9 to 8.6 and is similar to the surface waters like glacier meltwater/fresh snow (6 to 8.6), natural springs (6.8 to 7.6) and headwaters of Ganga (7.3 to 8.2). Therefore, it indicates the identical source of water in the region (Fig. 3A). The mouth temperature of the water in geothermal systems varies from 26 to 93 °C. The temperature range for surface waters (glacier meltwater, cold springs and river waters) was 2 to 21 °C (Tables 1 and 2 and S3 and Fig. 3B). Electrical conductivity (EC) of waters in geothermal systems varies from 340 to 4950 µS, while that for river waters, snow/glacier meltwater and cold springs varies from 59 to 271

Table 1 Details of samples collected and their in situ and laboratory measurements

Sr. no	Sample ID and name	Altitude (m asl)	Latitude (N)	Longitude (E)	Mouth temp. (°C)	pH	EC (µS/Cm)	Cl (µE)	$\delta^{18}O‰_{(vsmow)}$	$\delta D‰_{(vsmow)}$	d-excess	$^{87}Sr/^{86}Sr$
01	HS-1, Taptkund	3089	30° 44′ 41″	79° 20′ 29″	55.6	7.3	2690	3469	–13.1	–95.4	9.4	0.763
02	HS-2, Khiroi	2973	30° 40′ 48″	79° 27′ 35″	57.8	8.5	340	221	–12.6	–86.7	14.1	0.759
03	HS-3, Bhapkund	2680	30°40′ 05″	79° 50′0 5″	44.7	8.1	359	152	–11.5	–78.9	13.1	0.750
04	HS-4, Joshimath	1953	30°29′ 02″	79° 39′ 02″	93.0	7.3	805	198	–10.5	–74.3	9.7	0.755
05	HS-5, Tapoban	1890	30°29′ 02″	79° 38′ 01″	45.6	6.2	368	95	–10.1	–68.1	12.7	0.766
06	HS-6, Birahi	1190	30° 24′ 31″	79° 23′ 19″	64.6	6.2	1190	3509	–8.3	–59.5	6.9	0.937
07	HS-7, Ganoi	1409	30° 28′ 58″	79° 29′ 03″	25.6	6.5	1310	328	–8.3	–57.1	9.3	0.821
08	HS-8, Langsi	1225	30° 29′ 47″	79° 28′ 36″	53.0	6.7	1007	650	–8.8	–59.6	10.8	0.771
09	HS-9, Helang	1210	30° 31′ 10″	79° 29′ 38″	60.9	6.2	755	260	–8.5	–59.2	8.8	0.736
10	HS-10, Gaurikund	1930	30° 39′ 26″	79° 01′ 39″	47.3	6.6	1029	540	–9.2	–60.1	13.5	0.756
11	HS-11, Gangnani	1900	30° 54′ 11″	78° 40′ 50″	61.0	6.7	1314	1702	–9.3	–63.5	10.9	0.786
12	HS-12, Jhaya	1808	30° 53′ 05″	78° 40′ 10″	44.1	8.6	525	1076	–9.3	–62.6	11.8	1.440
13	HS-13, Bhukki	1730	30° 50′ 00″	78° 39′ 05″	52.0	6.5	1751	3752	–9.0	–61.5	10.5	0.803
14	HS-14, Thirang	1640	30° 50′ 54″	78° 38′ 08″	52.2	6.4	1480	2029	–8.8	–59.4	11.0	0.773
15	HS-15, Matli	1062	30° 44′ 16″	78° 23′ 20″	29.4	7.2	1372	5492	–7.5	–47.2	12.8	0.873
16	HS-16, Kotimanep	1429	30° 53′ 17″	78° 14′ 25″	35.0	5.9	1637	10,516	–8.6	–56.0	12.8	0.734
17	HS-17,Yamunotri	3070	30° 59′ 58″	78° 27′ 46″	84.3	7.1	1060	4226	–8.4	–56.6	10.6	1.140
18	HS-18, Jankichatti	2568	30° 58′ 39″	78° 26′ 24″	28.8	6.6	4950	21,986	–9.5	–56.6	11.5	0.763
19	HS-19, Banas	2210	30° 57′ 34″	78° 24′ 38″	70.0	6.1	440	617	–8.8	–60.4	10.0	0.759
20	HS-20, Wozari	1630	30° 54′ 24″	78° 20′ 14″	54.8	6.1	2030	4674	–9.7	–65.4	12.2	0.750
21	RW-1	3089	30° 44′ 41″	79° 20′ 29″	4.5	7.3	78	12	–14.3	–97.6	16.8	0.730
22	RW-2	3089	30° 44′ 45″	79° 20′ 30″	4.5	7.3	71	14	–14.2	–97.4	16.2	0.726
23	RW-4	1800	30° 40′ 00″	79° 50′ 00″	6.2	7.5	248	13	–13.0	–88.6	15.4	0.725
24	RW-5	1468	30° 29′ 34″	79° 37′ 49″	9.8	7.6	59	7	–12.8	–91.0	11.4	0.710
25	RW-6	1190	30° 33′ 47″	79° 34′ 35″	15.0	8.2	271	23	–11.6	–79.0	13.8	0.720
26	RW-8	2148	30° 24′ 31″	79° 23′ 19″	5.3	8.2	174	40	–10.4	–69.0	14.2	
27	RW-9	3070	30° 29′ 47″	79° 28′ 36″	1.8	8.0	81	30	–12.3	–85.0	13.4	
28	RW-10	2210	30° 57′ 49″	78° 41′ 48″	8.1	7.6	146	22	–10.7	–68.0	17.6	

Table 2 Details of samples of snowfall, glacier ice, meltwater, river water and rainfall collected for this study and their measurements

Sr. no	Sample ID	Nature of sample	Location	Latitude/ longitude	Altitude (m asl)	T (°C)	pH	EC (µS/Cm)	Cl (µE)	$^{18}O‰$	D‰	*d-excess*
1	S-01	Fresh snow	Dokriani Glacier, May 2013	30°, 86.275′N/ 78°, 80.235′E	4068		6.2	5	20	–13.0	–86.0	18
2	S-02				4068		6.0	7	7	–13.5	–91.0	17
3	S-03				4068		6.1	7	5	–13.7	–91.0	18.6
5	G.I	Glacier ice		30°, 86.335′N/ 78°, 80.248′E	4068		6.5	5	4	–13.7	–95.0	14.6
6	MW-1	Meltwater	Din Gad stream, May 19, 2013	30°, 51.573′N/ 78°, 47.395′E	3810	4.0	8.6	91	8	–14.6	–100.0	16.8
7	MW-2		Din Gad stream, May 20, 2013		3810	4.0	8.5	83	10	–11.4	–80.0	11.2
8	MW-3		Din Gad stream, May 21, 2013		3810	5.0	8.4	70	7	–10.7	–76.0	9.6
9	MW-4		Din Gad stream at Tela, May 17, 2013	30°, 15.098′N/ 78°, 41.283′E	2100	6.0	8.2	57	12	–11.1	–77.0	11.8
10	MW-5		Bhagirathi at Bhojwasa, Gaumukh, Sept 9, 2014	30.935°N/ 79.069°E	3760	4.0	6.6	70	2	–15.11	–110.8	10.08
11	MW-6		Bhagirathi at Bhojwasa, Gaumukh, Sept 11, 2014	30.935°N/ 79.069°E	3760	4.0	6.7	60	2	–15.6	–116.3	8.5
12	RW-11	River water	Bhagirathi at Uttarkashi	30°, 43′, 83.2″N/ 78°, 26′,87.3″E	1700	11.0	8.0	117	38	–10.8	–75.0	11.4
13	RW-12		Bhagirathi at Gangotri, Sept 12, 2017	30.935°N/ 79.069°E	3760	12.0	6.7	122	2	–15.6	–114.6	10.2
14	RIW-4	Rainfall	Dokriani Glacier, May 2010	30°, 51.573′N/ 78°, 47.395′E	3810					–8.99	–59.0	12.92
15	RIW-5		Dokriani Glacier, July 2010	30°, 51.573′N/ 78°, 47.395′E	3810					–15.65	–115.0	10.2
16	RIW-6		Dokriani Glacier, May 2011	30°, 51.573′N/ 78°, 47.395′E	3810					–8.88	–61.0	10.04
17	RIW-7		Dokriani Glacier, July 2011	30°, 51.573′N/ 78°, 47.395′E	3810					–10.7	–72.0	13.6

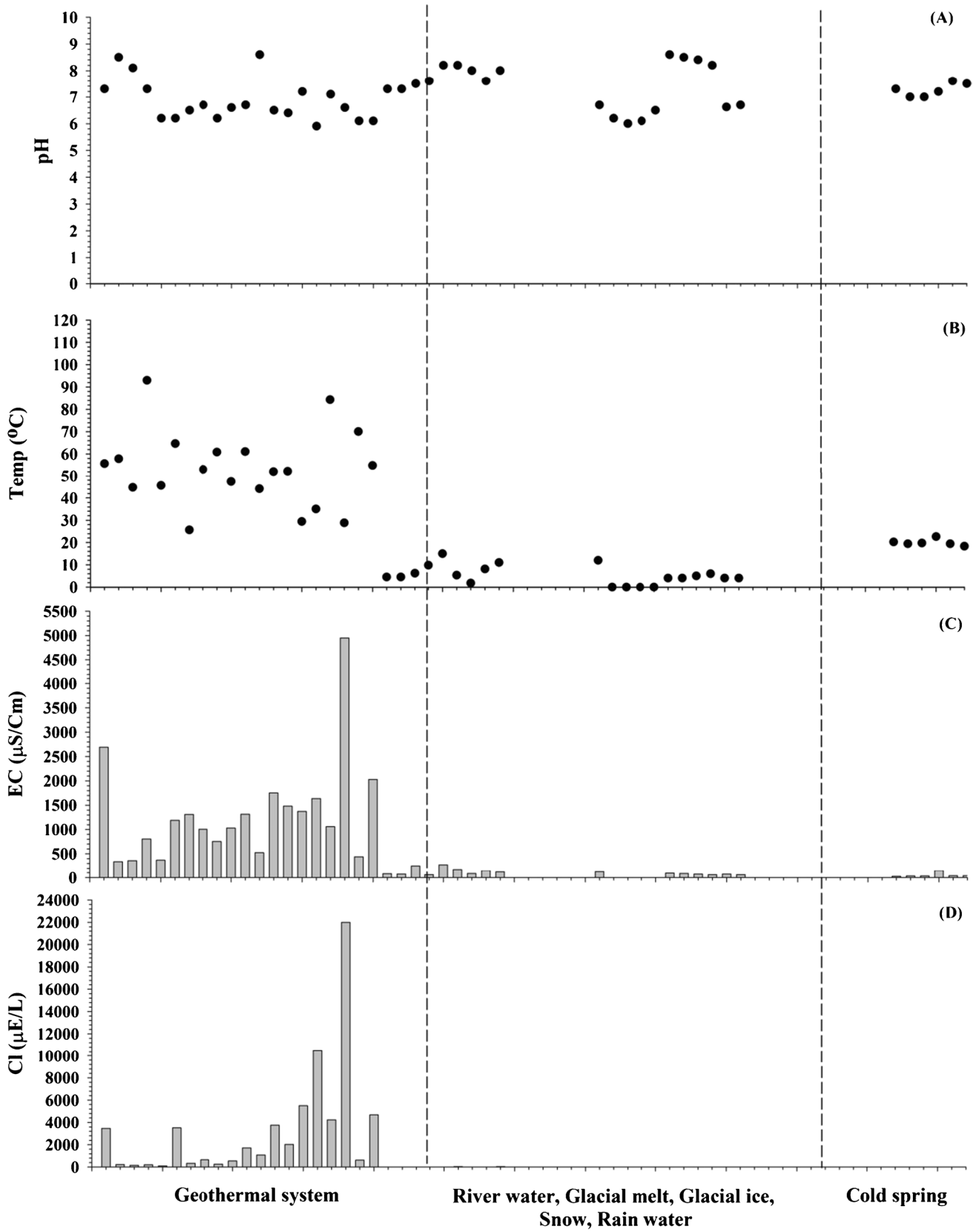

Fig. 3 Distribution and variability of a pH, b temperature, c electrical conductivity and d chloride in different waters of Garhwal Himalaya

µS, 5 to 122 µS and 24 to 311 µS, respectively (Fig. 3C). The EC of geothermal systems is higher by an order of magnitude as they are expressions of rock-water interaction at moderate to high temperatures.

Variability in chloride (Cl^-) and dissolved silica (SiO_2)

Hydro-geochemical analysis of geothermal systems is extensively applied as a fundamental method in distinguishing geothermal reservoirs and their evolution (Fournier 1981; Nicholson 1993). Concentrations of chloride and dissolved silica of geothermal systems, river waters, cold springs and glacial meltwater are available in Tables 1 and 2 and S3. The concentration of Cl^- in geothermal systems, river waters and cold springs varies from 95 to 21,986 µE/L, 7 to 40 µE/L and 6 to 274 µE/L, respectively, and the average is 3274 µE/L, 20 µE/L and 105 µE/L, respectively. The concentration of Cl^- in fresh snow and glacial meltwater varies from 2 to 38 µE/L, with an average of 10 µE/L (Fig. 3D). Cl^- is a major soluble ion of natural waters and does not precipitate except under evaporation and freezing processes. These conductive ions are derived from dissolved salts and inorganic materials such as alkalis, chlorides, sulphides and carbonate compounds (Miller et al. 1988). The high concentration of Cl^- indicates rock-water interaction in the deep reservoir, where conductive cooling and mixing are low. Low Cl^- values may specify the boundary and modern underground water interference to the geothermal system (Nicholson 1993). The observed variation in $\delta^{18}O$ of all geothermal systems is related to their altitude, while the concentration of Cl^- is relatively the same for all these systems. The variations in the $\delta^{18}O$ and chloride (Cl^-) are not by the effect of diverse evapo-concentrations or steam separation and are from the elevation difference of geothermal water recharge and sources of dissolved Cl^-, respectively (Tan et al. 2014; Tiwari et al. 2016a).

Dissolved silica (SiO_2) is a vital component of all geothermal fluids. The solubility of silica polymorphs (amorphous silica, opal, quartz, cristobalite and chalcedony) and other silicate minerals controls its concentration. The abundance of dissolved SiO_2 in geothermal systems and river waters varies from 380 to 2040 µE/L and 159 to 255 µE/L, respectively. The average dissolved SiO_2 in geothermal systems and river waters is 1399 µE/L and 205 µE/L, respectively (Table 1). The results strongly advocate that the surface waters infiltrate deep into the ground, possibly interacting with the silicates in the clayey level or minerals of volcanic rocks (Fig. 4A).

Variability in stable isotopic data ($\delta^{18}O$‰, δD ‰) and identification of the water source

Stable isotopes of water have been used as proxies to unearth the recharge source of geothermal systems in this study. The ratios of stable isotopes of ($\delta^{18}O$, δD) of all the water samples are shown in Tables 1, 2 and S3, whereas their variations are given in Fig. 4B and C. The ratio of stable isotopes of water ($\delta^{18}O$, δD) has an average of –9.4‰ and –65.2‰ in geothermal systems, –12.4‰ and –80.2‰ in river waters and –12.6‰ and –88.7‰ in the rain, fresh snow, glacial ice and meltwater of Dokriani Glacier. The cold springs of the Garhwal region have an average of –7.4‰ and –53.1‰. Similar values of stable isotopes of water in high-altitude rainfall, snowfall and glacial meltwater have been reported for Chorabari and Dokriani glaciers (Kumar et al. 2018; Verma et al. 2018). The range of stable isotopes of water in geothermal systems is covered by different waters like high-altitude rainfall, snowfall and glacial meltwater.

Geothermal systems may integrate waters from diverse sources, which could be resolved using stable isotopes of water. Friedman (1970) first reported the dominance of the meteoric component in geothermal systems by observing δD values; however, a better understanding came through the combined measurements of $\delta^{18}O$ and δD (Craig 1963). The equilibrium fractionations describe the relationship between $\delta^{18}O$ and δD composition in natural waters (Craig 1961a; Dansgaard 1964; Rozanski et al. 1993). Several studies led to the establishment of a Global Meteoric Water Line (GMWL) that is a relation between $\delta^{18}O$ and δD of precipitation from various parts of the world, having a slope of 8 and intercept of 10, which is described as "$\delta D = 8 * \delta^{18}O + 10$". In contrast, $\delta^{18}O$ and δD relationship at a regional or local scale is known as the Local Meteoric Water Line (LMWL). The intercept and slope may vary as a function of the location, seasonality and occurrences of extreme events. The "deuterium excess" or "d-excess" in precipitation is the intercept of the GMWL. It provides a measure of non-equilibrium effects (Dansgaard 1964) and indicates the environmental circumstances during phase transfer under a non-equilibrium environment.

The δD values of geothermal systems lie close to the local meteoric water, while $\delta^{18}O$ values are enriched. This shift in the $\delta^{18}O$ but not in δD of meteoric water can help understand the hydrothermal interactions at depths. Geothermal systems and volcanic landscapes have fractures and crevices through which rainfall penetrates the earth and goes to a certain depth prior to interacting with hot rocks and getting back to the surface. During this process, oxygen from the meteoric water endures exchange reactions with source rocks (crystalline igneous/carbonates), having enriched $\delta^{18}O$ in contrast with meteoric waters. Therefore, it would augment the enrichment of $\delta^{18}O$ in the water and depletes the $\delta^{18}O$ in the rock. However, there is very little hydrogen in igneous and carbonate rocks for exchange during this process, and the δD composition of water is unaltered. In such a situation, it forces the water line to the right side of the LMWL (Witcher et al. 2004).

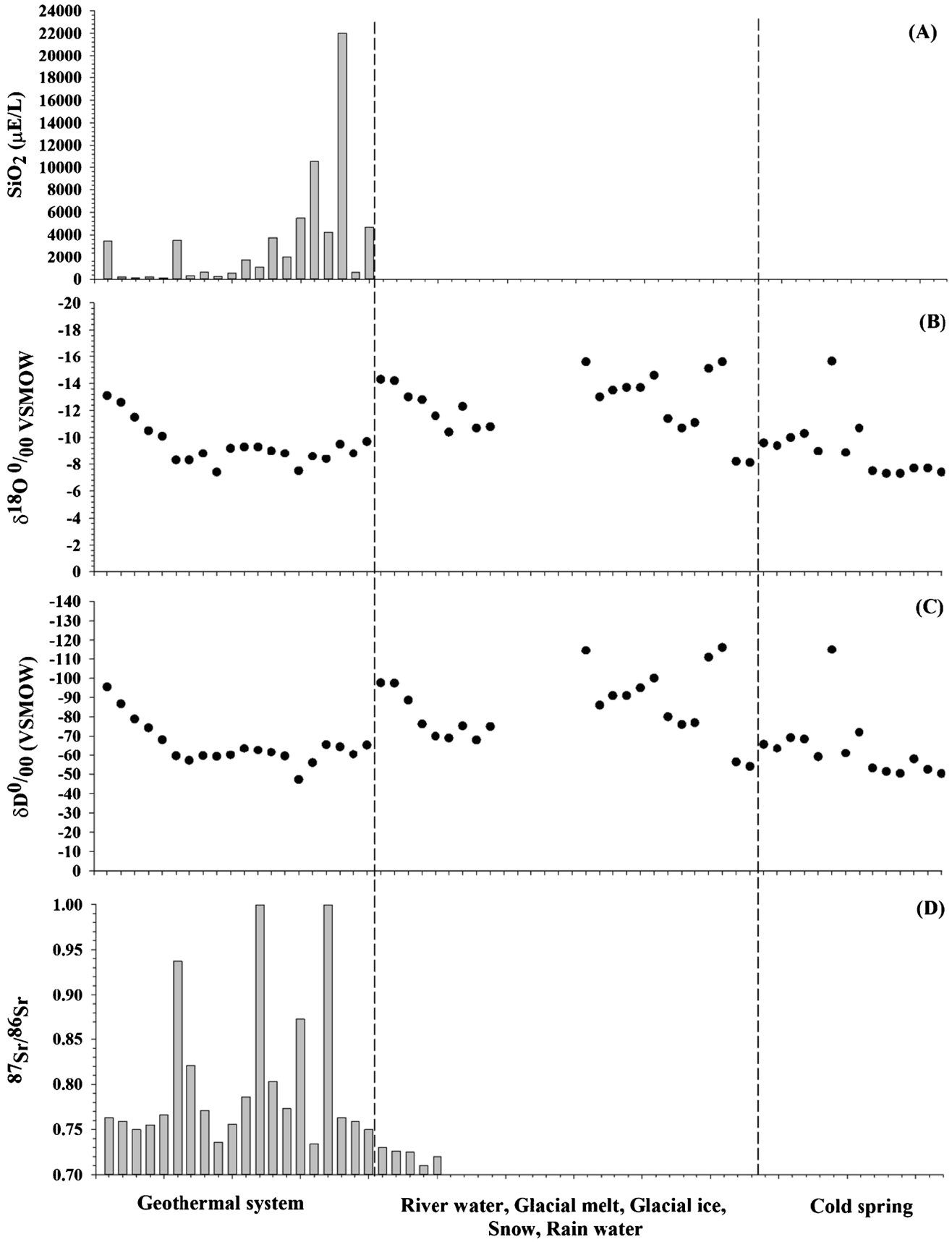

Fig. 4 Distribution and variability of a dissolved silica (SiO_2), b$\delta^{18}O$, c δH and d $^{87}Sr/^{86}Sr$ ratio in different waters of Garhwal Himalaya

Therefore, the $\delta^{18}O$ and δD relationship of geothermal waters is useful to study the altitude effect and source of water in geothermal systems.

The LMWL for geothermal systems, river water, meltwater, rainfall and fresh snow in the study region lies over or close to the GMWL with varied slope and intercepts (Fig. 5). D-excess in geothermal systems in the study area ranges from 6.9 to 19.4, with a mean of 13.2 ± 6.2 (Tables 1 and S4). The d-excess of these systems is quite similar to glacial meltwater, high-altitude rainfall and snowfall in UGB (Ramesh and Sarin 1992; Bartarya et al. 1995; Dalai et al. 2002; Kumar et al. 2018; Verma et al. 2018). The slope and intercept for geothermal systems are similar to glacial meltwater, high-altitude rainfall and snowfall in UGB. The slope, intercept and d-excess of cold springs, Yamuna and Indus Rivers are different (Fig. 6), because of the different climates, location and altitude of these systems. Therefore, the slope, d-excess and intercept of geothermal systems indicate that high-altitude rainfall, snowfall and meltwater from glaciers are the foremost source of recharge of these geothermal systems. Although the geothermal fluids exhibit meteoric origin, chemical compositions and variations indicate the likelihood of a small (5–10%) but noteworthy addition of the magmatic or deeper component (Nicholson 1993; Barbier 2002; Tiwari 2014).

Identification of the source of the geothermal fluid using $^{87}Sr/^{86}$ Sr ratio

The Himalayan Rivers contribute significantly to the Sr isotope mass balance of the modern oceans and have high Sr and elevated $^{87}Sr/^{86}Sr$ among the world rivers (Edmond 1992). The chief source of radiogenic Sr flux in Himalayan Rivers is from processes like weathering of different silicate phases and radiogenic carbonates (Palmer and Edmond 1989; Derry and France-Lanord 1996; Quade et al. 1997; Blum et al. 1998; Singh et al. 1998; Galy and France-Lanord 1999; Krishnaswami 1999; English et al. 2000). Radiogenic isotope ($^{87}Sr/^{86}Sr$) ratios of all the water samples are given in Table 1, and their variations are shown in Fig. 4D. The radiogenic isotope ratio of strontium ($^{87}Sr/^{86}Sr$) varies from 0.73 to 1.44‰, with an average of 0.83‰ in geothermal systems. In the associated river waters, the ratio varies from 0.71 to 0.73‰, with an average of 0.72‰ (Fig. 4D), indicating different water–rock reactions between them. These results reveal that the river waters did not infiltrate deep into the thermal reservoirs and are not the recharge source of geothermal systems (Tan et al. 2014; Zhao et al. 2003). Several previous studies suggest that geothermal systems contribute a significant amount of radiogenic strontium to the Himalayan Rivers and deliver up to 30% of the Sr flux to rivers (Evans et al. 2001). Therefore, the Earth's internal fluids/magma/heat source interacts with the water at depths for transferring the heat and radiogenic $^{87}Sr/^{86}Sr$ to the water in geothermal systems.

Circulation of water in geothermal systems

The recharge source of geothermal systems originates at a high altitude, which is beneficial to understand the movement of geothermal water and estimate the recharge altitude.

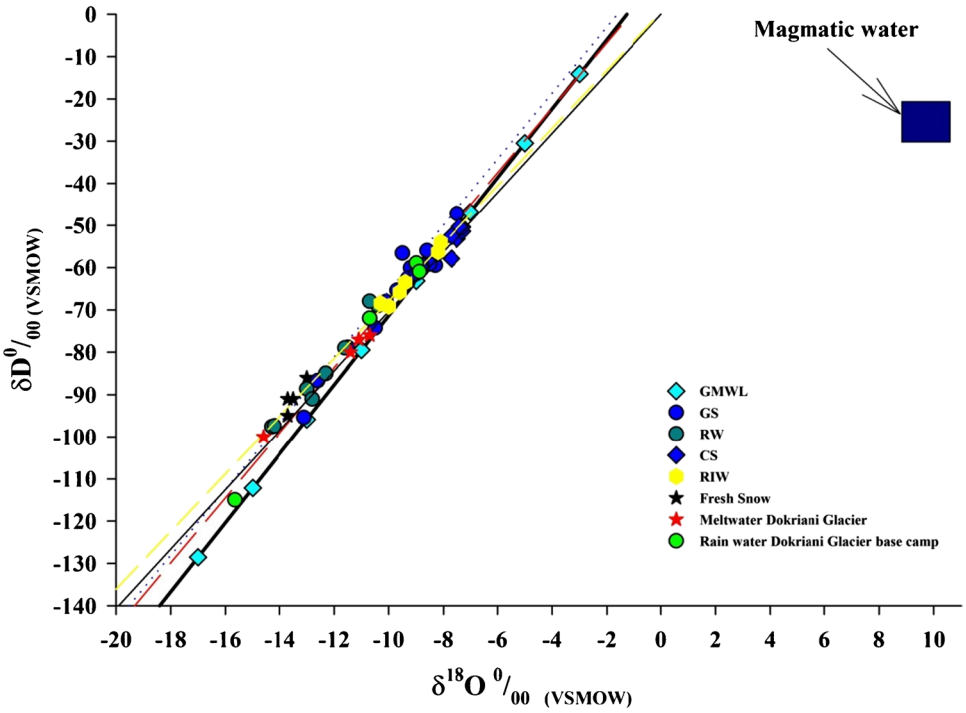

Fig. 5 Meteoric water line for different waters of Garhwal Himalaya and comparison with GMWL

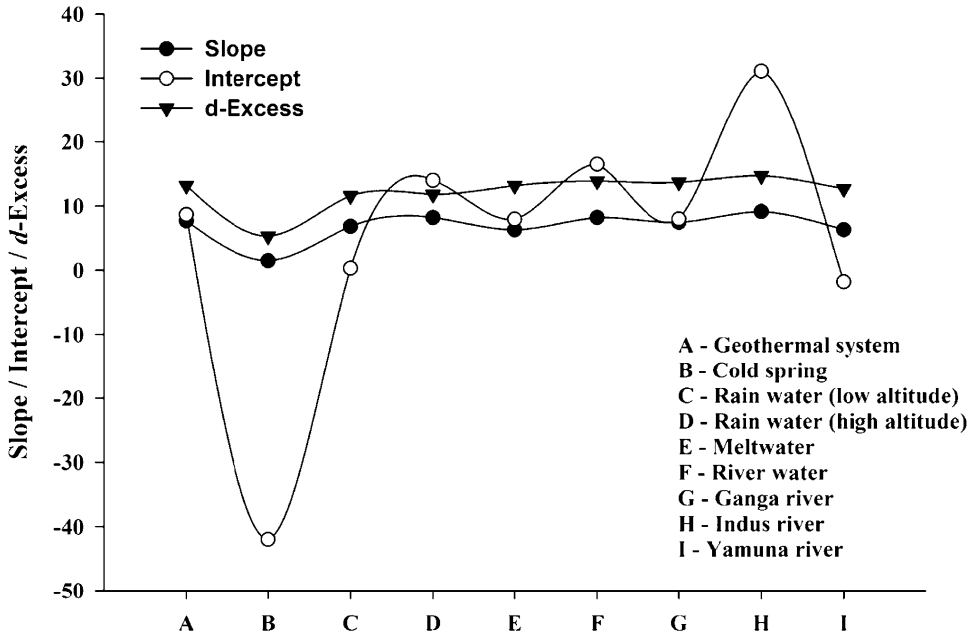

Fig. 6 Variation in slope, intercept and d-excess of different water components

The isotopic composition of precipitation varies with the altitude of the sampling location (Yurtsever and Gat 1981; Clark and Fritz 1997) and is known as the "altitude effect". As air masses lift orographically, they cool and cause precipitation which is enriched in heavier isotopes. The next phase of precipitation condensing from the residual cloud mass at a higher altitude would deplete in heavy isotopes; this process progressively increases with altitude. Therefore, the precipitation history, topography and perceptible moisture remaining in the cloud control the altitude effect. For ^{18}O, the depletion varies between –0.15 and –0.5‰ per 100 m rise in altitude, with a corresponding decrease of –1 to –4‰ for ^{2}H (Yu et al. 1984; Schotterer et al. 1997; Wright et al. 2001; Blasch and Bryson 2007). Rayleigh distillation manifests continental and altitude effects on a large spatial scale due to cloud migration and the continuous withdrawal of water from the ascending clouds. Krishnamurthy and Bhattacharya (1991) have observed the continental effect in precipitation over northern India. The rivers also reflect the altitude effect associated with precipitation, as precipitation is the dominant water source in rivers. However, river water is likely to be more depleted relative to precipitation at that site as it represents a mixture of various waters from streams draining from higher altitudes up to the site.

Geothermal systems of the Garhwal region indicate an altitude effect in $\delta^{18}O$ and δD. The altitude of the geothermal systems of Garhwal Himalaya varies from ~ 1160 to 3089 m asl, and the value of $\delta^{18}O$ varies from –7.5‰ to –13.1‰ (Table 1). The altitude effect for the geothermal systems and the UGB is –0.2 ± 0.025‰ per 100 m and –0.2 ± 0.006‰ per 100 m (Fig. 7). These lie within the values reported in earlier studies in the Garhwal Himalaya (Table 3). Some geothermal systems have an altitude higher than the River and have depleted isotopic ratios than the river waters (Table 1). The geothermal systems which have a lower elevation than the river show enriched ratios although rain and glacial meltwater from an altitude of 3810 m asl demonstrate similar isotopic values as water in geothermal systems. The results for the UGB, Gaula and Yamuna rivers in Garhwal Himalaya (Ramesh and Sarin 1992; Bartarya et al. 1995; Dalai et al. 2002) and Seti and the Kali Gandaki watersheds in Nepal (Garzione et al. 2000a, b) also show the altitude effect in $\delta^{18}O$ and δD values of rivers (Table 3). The precipitation collected from 11 sites between 250 and 3250 m asl at Mount Meager, a Quaternary volcano in western British Columbia, shows an altitude effect of –0.25‰ per 100 m (Clark et al. 1982) which provided evidence for the recharge environment of the geothermal groundwater. A gradient of –0.2‰ per 100 m for $\delta^{18}O$ prevails in the Jura Mountains of northern Switzerland (Siegenthaler and Matter 1983). A schematic physical model of the recharge process for geothermal systems of the Garhwal region is shown in Fig. 8. The top panel of the physical model (Fig. 8A) represents the process of infiltration of the meteoric waters (rainfall, snow and glacier melt) from high altitude into the ground through the faults/thrusts of the region and subsequent heating from the underlying heat source in the MCT zone and is released as geothermal springs. The Moho is the boundary between the crust and the mantle in the earth. This is a depth where seismic waves change velocity and there is also a change in chemical composition. The resistivity data (Fig. 8B) in the lower panel of the physical model indicates very low resistivity values in the MCT zone at comparatively low depths (5–20 km) indicating the presence of partial melt

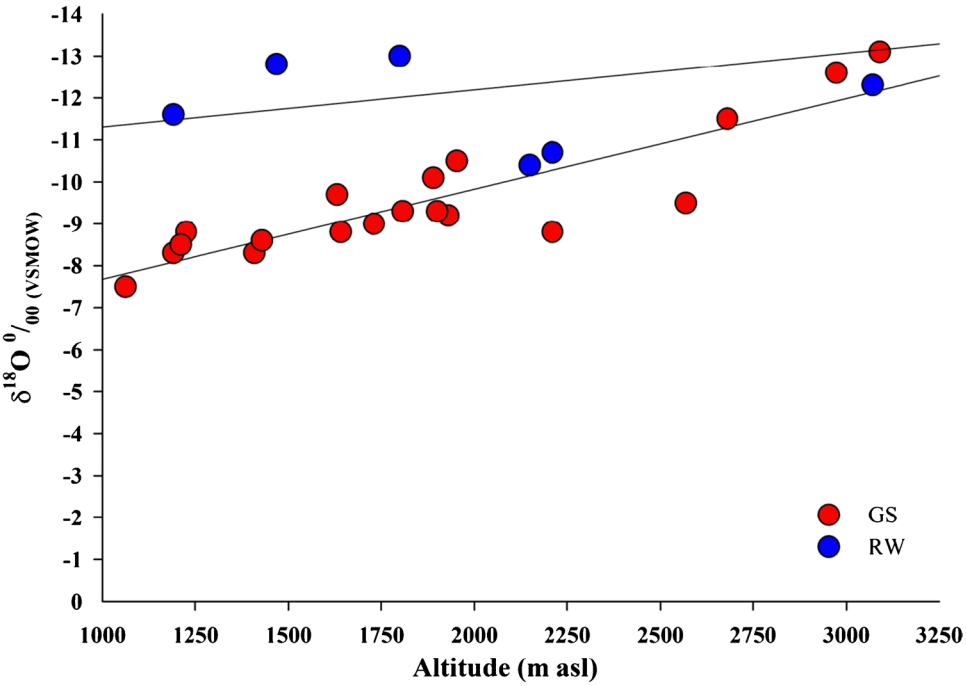

Fig. 7 Altitude effect in river water (RW) and geothermal systems (GS) of Garhwal Himalaya

Table 3 Altitude effect in geothermal systems, cold springs, rainfall and rivers in the Himalayan region

Site name	Region	Year/month	No. of samples	Altitude effect	Intercept	R^2	*P*	Reference
Geothermal systems	Garhwal Himalaya	2010	20	–0.2 ± 0.025	–6.38 ± 0.75	0.80	0001	*This study*
Ganga River		2010	10	–0.2 ± 0.006	–9.37 ± 1.6	0.60	0003	*This study*
Cold springs		2009	11	–0.2 ± 0.047	–7.25 ± 0.50	0.10	0001	Shivanna et al. 2008
Low altitude rain		2009	3	–0.4 ± 0.015	–4.58 ± 1.52	0.90	0.204	
Yamuna River		June	10	–0.09 ± 0.01	–7.4 ± 0.1	–0.84	NA	Dalai et al. (2002)
		Oct 1998	6	–0.11 ± 0.01	–7.7 ± 0.1	–0.86	NA	
		June, Oct 1999	16	–0.11 ± 0.01	–7.3 ± 0.1	–0.85	NA	
Ganga River		Apr 1990	5	–0.19 ± 0.01	–8.4 ± 0.2	–0.98	NA	Ramesh and Sarin 1992
Gaula River		Feb, June, Oct, 1983–1985	30	–0.14 ± 0.01	–63 ± 0.2	–0.69	NA	Bartarya et al. 1995
Indus River	Ladakh	Aug 1999	6	–0.09 ± 0.01	–12.1 ± 0.4	–0.58	NA	Pande et al. 2000
Seti River	Nepal	March/Apr 1999	12	–0.29 ± 0.03	–5.9 ± 0.2	–0.96	NA	Garzione et al. (2000a, b)
Kali Gandaki River	Nepal	Sept, Oct 1999	38	–0.29 ± 0.01	–6.8 ± 0.3	–0.96	NA	

or metamorphic fluids (Caldwell et al. 2013). These fluids are the primary heat source for the geothermal systems and provide the thermal gradient for heating the meteoric waters. Therefore, the meteoric waters infiltrate to a shallow depth and are heated and released as geothermal waters.

Geothermal systems: a permanent source of Earth's internal heat

The data of the mouth temperature of the geothermal systems of Garhwal Himalaya since 1975–1994 (Geological Survey of India) and 2010–2016 (this study) signify that the mouth temperatures of these systems remain the same over the last four decades with an error of < 5% (Fig. 9 and Table S5). The extent of dissolution and precipitation of different substances and their solute characteristics depend upon the temperature and water–rock interactions with thermal fluids extracted from the deep reservoir. Hence, it is essential to understand the temperature-induced process and infer the character of the thermal reservoirs. Field observations, chemical composition and physical parameters of these geothermal systems show no temporal variation in

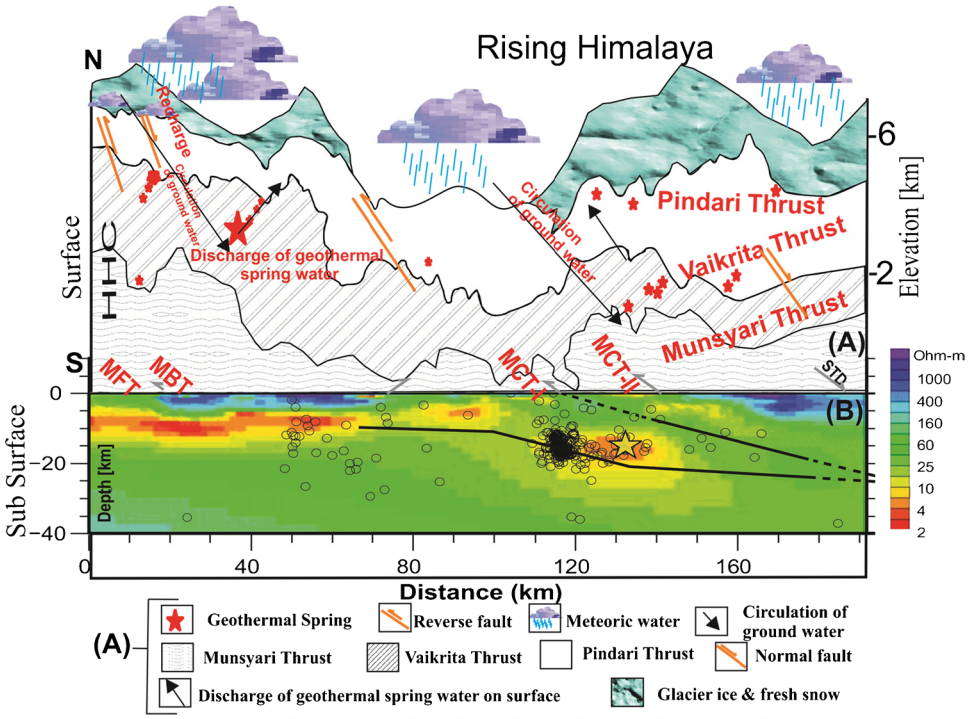

(B) Background is the resistivity along the study area adopted from [Caldwell et al., 2013].

Fig. 8 A physical model depicting the process of recharge of geothermal systems (**a**) and resistivity data (**b**) for Garhwal Himalaya

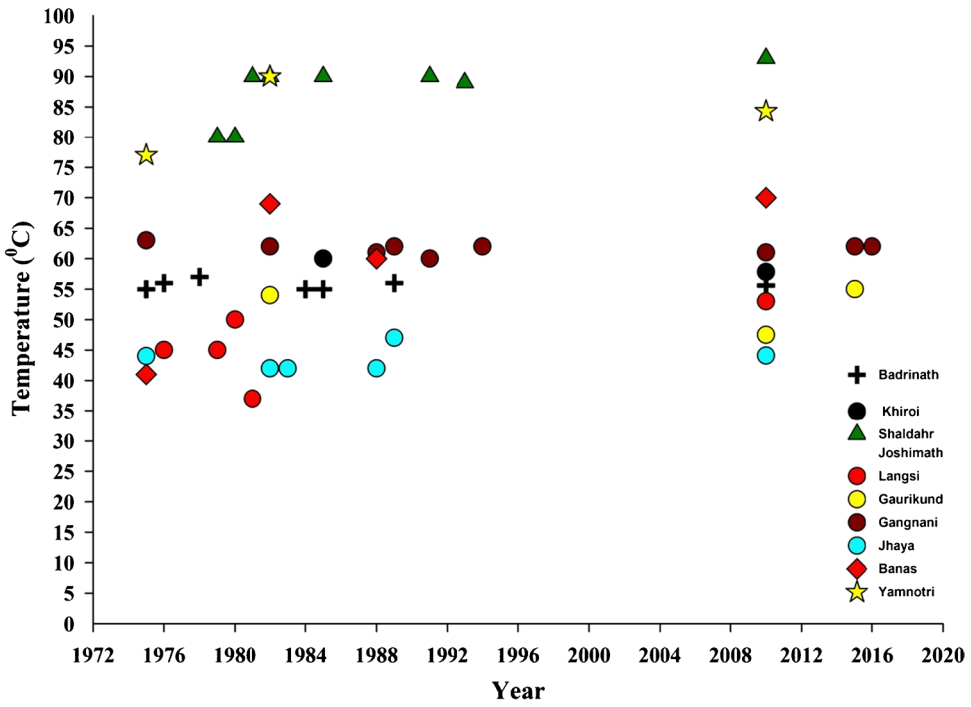

Fig. 9 Variation in the water temperature at the mouth of different geothermal systems of Garhwal Himalaya

their constituent (Gupta and Agarwal 2001; Tiwari et al. 2016a). Previous studies in other parts of the Himalaya also reveal similar results (Piao et al. 2010; Meng et al. 2012; Tan et al. 2014), thus indicating that geothermal systems act as a profuse, continuous source of energy which is dependent on post-tertiary granite intrusions for the high thermal gradient (> 100 °C/Km) and heat flow (> 468 mW/m^2) (Chandrasekharam and Chandrasekhar 2000).

Further, the discharge of geothermal systems has remained more or less unchanged over the period between

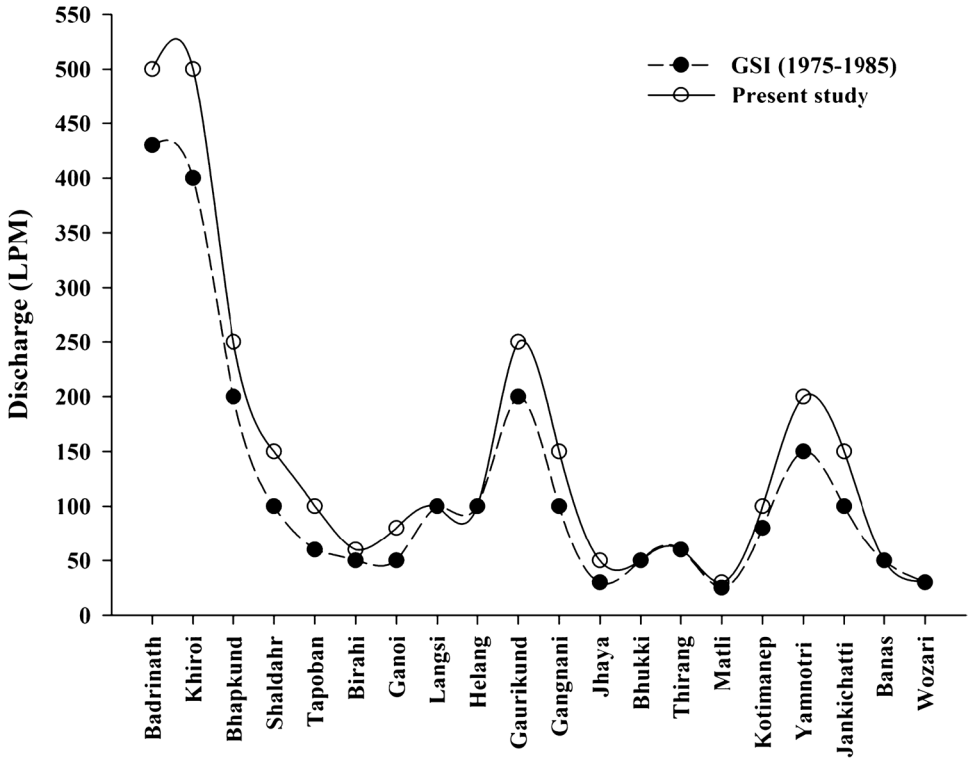

Fig. 10 Variation in discharge from geothermal systems of Garhwal Himalaya

1975 and 2016 (Fig. 10), with small variations observed due to changes in the season of sampling or increased snow and glacier meltwater in the Garhwal region. Therefore, the recharge of geothermal systems is a continuous process, and availability of meteoric waters like high-altitude precipitation (rainfall and snowfall) and glacier melt will keep these geothermal systems healthy. It is a comparatively clean and renewable energy resource and hence becoming a preferred choice for alternative energy. In India, the estimated potential to generate ~ 10,600 MWe of power (Craig et al. 2013) using the latest technologies in geothermal systems is still unutilised.

Conclusions

This study concludes that the different geothermal systems of Garhwal Himalaya have high electrical conductivity (EC) by an order of magnitude than the background due to rock-water interactions at moderate to high temperatures. The enriched Cl^- in the geothermal systems may be derived from the chloride phase present in the metamorphic crustal fluid. The radiogenic $^{87}Sr/^{86}Sr$ data reveals that river water is not the recharge source of geothermal waters.

Based on the isotopic composition ($\delta^{18}O$ and δD), slope, d-excess and intercept of the LMWL of geothermal waters, it is evident that meteoric waters (rainfall, snow and glacier melt) are the principal recharge source of geothermal systems in Garhwal Himalaya. Therefore, it is important to monitor the seasonal and annual precipitation (rainfall and snowfall) and the state of Himalayan glaciers to understand the sustainability of these geothermal systems for utilisation of the communities living in downstream.

The discharge and mouth temperature of the water of these geothermal systems remains unchanged, thus indicating that these springs are a continuous source of energy and their potential can be harnessed for the generation of electricity and internal heating of buildings in the vicinity as done by several Scandinavian countries. Further, various studies have indicated the presence of heavy metals and carcinogens in the waters of the geothermal systems; thus, these waters should be carefully utilised for domestic and agricultural purposes.

Supplementary Information The online version contains supplementary material available at https://doi.org/10.1007/s12517-021-08679-8.

Acknowledgements The authors would like to thank the director of Wadia Institute of Himalayan Geology, Dehradun, for providing the facilities to conduct this study. This work was funded by the Department of Science and Technology (DST), Government of India. This work carries Wadia Institute of Himalayan Geology contribution No. WIHG/0106.

Declarations

Conflict of interest The authors declare that they have no competing interests.

References

Aggarwal NC, Kumar G (1973) Geology of the upper Bhagirathi and Yamuna Valley. Uttarkashi District Him Geol 3:2–23

Auden JB (1937) The structure of the Himalaya in Garhwal. Records Geological Survey of India 71(4):407–433

Azeez KKA, Harinarayana T (2007) Magnetotelluric evidence of potential geothermal resource in Puga, Ladakh, NW Himalaya. Curr Sci 93:323–329

Barbier E (2002) Geothermal energy technology and current status: an overview. Renewable Sustainable Energy Rev 6(1–2):3–65

Bartarya SK, Bhattacharya SK, Ramesh R, Somayajulu BLK (1995) $\delta^{18}O$ and δD systematics in the surficial waters of the Gaula catchment area, Kumaun Himalaya. India J Hydrol 167:369–379

Beaumont C, Muñoz JA, Hamilton J, Fullsack P (2000) Factors controlling the Alpine evolution of the central Pyrenees inferred from a comparison of observations and geodynamical models J Geophys Res Solid. Earth 105(B4):8121–8145

Becker JA, Bickle MJ, Galy A, Holland TJB (2008) Himalayan metamorphic CO2 fluxes: quantitative constraints from hydrothermal springs. Earth Planet Sci Lett 265:616–629

Bhattacharya AR (1985) A phenomenon of unusual flattening in natural folds associated with a Himalayan thrust. Geol Mijnbouw 64:159–165

Bilham R, Larson K, Freymuller J (1997) Indo-Asian convergence rates in the Nepal Himalaya. Nat 386:61–66

Blasch KW, Bryson JR (2007) Distinguishing sources of ground water recharge by using δ2H and δ18O. Groundwater 45(3):294–308

Blum JD, Gazis CA, Jacobson AD, Page Chamberlain C (1998) Carbonate versus silicate weathering in the Raikhot watershed within the High Himalayan Crystalline Series. Geol 26(5):411–414

Bruijnzeel LA, Bremmer CN (1989) Highland-lowland interactions in the Ganges Brahmaputra river basin: a review of published literature

Caldwell WB, Klemperer SL, Lawrence JF, Rai SS (2013) Characterizing the Main Himalayan Thrust in the Garhwal Himalaya, India with receiver function CCP stacking. Earth Planet Sci Lett 367:15–27

Chandrajith R, Barth JA, Subasinghe ND, Merten D, Dissanayake CB (2012) Geochemical and isotope characterization of geothermal spring waters in Sri Lanka: evidence for steeper than expected geothermal gradients. J Hydrol 476:360–369

Chandrasekharam D, Chandrasekhar V (2000) Geothermal energy resources of India: country update. In: Proceedings World Geothermal Congress, pp 133–145

Chatterjee J, Singh SK (2012) 87Sr/86Sr and major ion composition of rainwater of Ahmedabad, India: sources of base cations. Atmos Environ 63:60–67

Choubey VM, Bist KS, Saini NK, Ramola RC (1999) Relation between soil-gas radon variation and the different lithotectonic units of Garhwal Himalaya. India Appl Radiat Isot 1(5):587–592

Cinti D, Pizzino L, Voltattorni N, Quattrocchi F, Walia V (2009) Geochemistry of thermal waters along fault segments in the Beas and Parbati valleys (north-west Himalaya, Himachal Pradesh) and in the Sohna town (Haryana). India Geochem J 43(2):65–76

Clark ID, Fritz P (1997) Environmental Isotopes in Hydrogeology 81:328

Clark ID, Fritz P, Michel FA, Souther JG (1982) Isotope hydrogeology and geothermometry of the Mount Meager geothermal area. Can J Earth Sci 19(7):1454–1473

Clayton RN, Friedman I, Graf DL, Mayeda TK, Meents WF, Shimp NF (1966) The origin of saline formation waters: 1. Isotopic Composition J Geophys Res 71(16):3869–3882

Craig H (1961a) Isotopic Variation in Meteoric Waters Sci 133:1702–1703

Craig H (1961b) Standard for reporting concentrations of deuterium and oxygen-18 in natural waters. Sci 133:1833–1834

Craig H (1963) The isotopic geochemistry of waters and carbon in geothermal areas. Nuclear Geology in Geothermal Areas, Spoleto, pp 17–53

Craig J, Absar A, Bhat G, Cadel G, Hafiz M, Hakhoo N, Kashkari R, Moore J, Ricchiuto TE, Thurow J, Thusu B (2013) Hot springs and the geothermal energy potential of Jammu & Kashmir State, N.W. Himalaya. India Earth Sci Rev 126:156–177

Dalai TK, Krishnaswami S, Sarin MM (2002) Major ion chemistry in the headwaters of the Yamuna River System: chemical weathering, its temperature dependence and CO_2 consumption in the Himalaya. Geochim Cosmochim Acta 66:3397–3416

Dansgaard W (1964) Stable isotopes in precipitation. Tellus 16(4):436–468

Derry LA, Evans MJ, Darling R, France-Lanord C (2009) Hydrothermal heat flow near the Main Central Thrust, central Nepal Himalaya. Earth Planet Sci Lett 286(1–2):101–109

Derry LA, France-Lanord C (1996) Neogene Himalayan weathering history and river87Sr86Sr: impact on the marine Sr record. Earth Planet Sci Lett 142(1–2):59–74

Edmond JM (1992) Himalayan tectonics, weathering processes, and the strontium isotope record in marine limestones. Sci 258(5088):1594–1597

English NB, Quade J, DeCelles PG, Garzione CN (2000) Geologic control of Sr and major element chemistry in Himalayan rivers. Nepal Geochim Cosmochim Acta 64(15):2549–2566

Evans MJ, Derry LA (2003) Geothermal fluxes of solutes, heat, and carbon to central Nepal rivers. Doctoral dissertation, Ph. D. thesis, Cornell Univ

Evans MJ, Derry LA, Anderson SP, France-Lanord C (2001) Hydrothermal source of radiogenic Sr to Himalayan rivers. Geol 29(9):803–806

Evans MJ, Derry LA, France-Lanord C (2004) Geothermal fluxes of alkalinity in the Narayani river system of central Nepal. Geochem Geophys Geosyst 5(8):1–21

Evans MJ, Derry LA, France-Lanord C (2008) Degassing of metamorphic carbon dioxide from the Nepal Himalaya. Geochem Geophys Geosyst 9(4):Q04021

Evans M J (2003) Geothermal fluxes of solutes, heat, and carbon to central Nepal rivers. Doctoral dissertation, Ph. D. thesis, Cornell Univ

Forster C, Smith L (1989) The influence of groundwater flow on thermal regimes in mountainous terrain: a model study J Geophys Res Solid. Earth 94(B7):9439–9451

Fournier RO (1981) Application of water geochemistry to geothermal exploration and reservoir engineering. In: Geothermal systems: principles and case histories, pp 109–143

Friedman I (1970) The isotopic chemistry of a travertine-depositing spring. Geochim Cosmochim Acta 34:1303–1315

G.S.I. (1991) Geothermal atlas of India. Geol Surv India Sp Pub 19:143

Galy A, France-Lanord C (1999) Weathering processes in the Ganges-Brahmaputra basin and the riverine alkalinity budget. Chem Geol 159:31–60

Gansser A (1964) Geology of the Himalayas

Garzione CN, Dettman DL, Quade J, DeCelles PG, Butler RF (2000a) High times on the Tibetan Plateau: paleoelevation of the Thakkhola graben. Nepal Geol 28:339–342

Garzione CN, Quade J, DeCelles PG, English NB (2000b) Predicting palaeoelevation of Tibet and the Himalaya from $\delta^{18}O$ vs. altitude gradients in meteoric waters across the Nepal Himalaya. Earth Planet Sci Lett 183:215–229

Gupta GK, Agarwal RK (2001) A compilation of data on chemical analyses of water and gas samples from geothermal fields

of northwest Himalaya and adjoining areas (no. 5). Director General, Geological Survey of India
Gupta HK, Roy S (2006) Geothermal energy: an alternative resource for the 21st century. Elsevier
Gururajan NS, Choudhuri BK (1999) Ductile thrusting, metamorphism and normal faulting in Dhauliganga Valley. Garhwal Himalaya Himal Geol 20(2):19–29
Gyanprakash, Raina CB (1975) Report on preliminary geothermal investigation of some hot springs of U.P., Himalaya. Unpublished, G.S.I, report
Harinarayana T, Abdul Azeez KK, Murthy DN, Veeraswamy K, Eknathrao SP, Manoj C, Naganjaneyulu K (2006) Exploration of geothermal structure in Puga geothermal field, Ladakh Himalayas, India, by magnetotelluric studies. J Appl Geophys 58(4):280–295
Harrison TM, Copeland P, Kidd WSF, Yin A (1992) Raising Tibet Sci 255:1663–1670
Harrison TM, Yin A, Ryerson FJ (1998) Orographic evolution of the Himalaya and Tibet. Oxf Monogr Geol Geophys 39:39–72
Heim A, Gansser A (1975) Central Himalaya: Geological observations of the Swiss expedition, 1936. 73, Hindustan Publishing Corporation (India)
Henry P, Le., Pichon, X., Goffe´, B. (1997) Kinematic, thermal and petrological model of the Himalayas; constraints related to metamorphism within the underthrust Indian crust and topographic elevation. Tectonophysics 273(1–2):31–56
Hochstein MP, Regenauer LK (1998) Heat generation associated with collision of two plates: the Himalayan geothermal belt. J Volcanol Geotherm Res 83(1–2):75–92
Ingebritsen SE, Galloway DL, Colvard EM, Sorey ML, Mariner RH (2001) Time-variation of hydrothermal discharge at selected sites in the western United States: implications for monitoring. J Volcanol Geotherm Res 111(1–4):1–23
Jenkin GRT, Craw D, Fallick AE (1994) Stable isotopic and fluid inclusion evidence for meteoric fluid infiltration into an active mountain belt; Alpine Schist. New Zealand J Metamorph Geol 12(4):429–444
Koons PO, Craw D (1991) Evolution of fluid driving forces and composition within collisional orogens. Geophys Res Lett 18(5):935–938
Koons PO, Craw D, Cox S, Upton P, Templeton A, Chamberlain CP (1998) Fluid flow during active oblique convergence: a southern Alps model from mechanical and geochemical observations. Geol 26:159–162
Krishnamurthy RV, Bhattacharya SK (1991) Stable oxygen and hydrogen isotope ratios in shallow groundwater from India and a study of the role of evapotranspiration in the Indian monsoon. Stable Isotope Geochemistry: A Tribute to Samuel Epstein 3:187–193
Krishnaswami S (1999) Silicate weathering in the Himalaya: role in contributing to major ions and radiogenic Sr to the Bay of Bengal. Ocean science, trends and future directions
Kumar A, Tiwari SK, Verma A, Gupta AK (2018) Tracing isotopic signatures (δD and δ 18 O) in precipitation and glacier melt over Chorabari Glacier-Hydroclimatic inferences for the Upper Ganga Basin (UGB), Garhwal Himalaya. J. Hydrol.: Reg. Stud 15:68–89
LeFort P (1975) Himalayas-collided range-present knowledge of continental arc: American Journal of Science, v
Manga M (1998) Advective heat transport by low-temperature discharge in the Oregon Cascades. Geol 26(9):799–802
Meng J, Wang C, Zhao X, Coe R, Li Y, Finn D (2012) India-Asia collision was at 24 N and 50 Ma: palaeomagnetic proof from southernmost Asia. Sci Rep 2(1):1–11
Miller RL, Bradford WL, Peters NE (1988) Specific conductance: theoretical considerations and application to analytical quality control, vol 142. US Government Printing Office. http://pubs.usgs.gov/wsp/2311/report.pdf
Molnar P (1987) Inversion profile of uplift rates for geometry of dip-slip faults at depth, with example from Alps and Himalaya. Ann Geophys 5(6):663–670
Newell DL, Jessup JM, Cottle MJ, Hilton RD, Sharp ZD (2008) Aqueous and isotope geochemistry of mineral springs along the southern margin of the Tibetan plateau: Implications for fluid sources and regional degassing of CO_2. Geochem Geophys Geosyst 9(8):Q08014
Nicholson K (1993) Geothermal fluids, chemistry and exploration techniques. Springer Science & Business Media
Palmer MR, Edmond JM (1989) The strontium isotope budget of the modern ocean. Earth Planet Sci Lett 92(1):11–26
Pande K, Padia JT, Ramesh R, Sharma KK (2000) Stable isotope systematics of surface water bodies in the Himalayan and Trans-Himalayan (Kashmir) region. J Eart Sys Sci 109(1):109–115
Paul SK (1998) Geology and tectonics of the Central Crystallines of northeastern Kumaun Himalaya. India J Nepal Geol Soc 18:151–167
Piao S, Ciais P, Huang Y, Shen Z, Peng S, Li J, Friedlingstein P (2010) The impacts of climate change on water resources and agriculture in China. Nat 467(7311):43–51
Quade J, Roe L, DeCelles PG, Ojha TP (1997) The late Neogene 87Sr/86Sr record of lowland Himalayan rivers. Sci 276(5320):1828–1831
Rai SK, Tiwari SK, Bartarya SK, Gupta AK (2015) Geothermal systems in the northwest Himalaya. Cur Sci 108(9):1597
Ramesh R, Sarin MM (1992) Stable isotope study of the Ganga (Ganges) river system. J Hydrol 139:49–62
Ramstein G, Fluteau F, Besse J, Joussaume S (1997) Effect of orogeny, plate motion and land-sea distribution on Eurasian climate change over the past 30 million years. Nat 386:788–795
Rawat G (2012) Electrical conductivity imaging of Uttarakhand Himalaya using MT method. PhD. Thesis. Indian Institute of Technology (IIT), Roorkee, India
Rawat G, Arora BR, Gupta PK (2014) Electrical resistivity cross-section across the Garhwal Himalaya: proxy to fluid-seismicity linkage. Tectonophysics 637:68–79
Roy AB, Valdiya KS (1988) Tectonometamorphic evolution of the Great Himalayan thrust sheets in Garhwal region. Kumaun Himalaya J Geol Soc Ind 32(2):106–124
Royden LH, Burchfiel BC, King RW, Wang E, Chen Z, Shen F, Liu Y (1997) Surface deformation and lower crustal flow in eastern Tibet. Sci 276:788–790
Rozanski K, Araguas-Araguas L, Gonfiantini R (1993) Isotopic patterns in modern global precipitation. Climate Change in Continental Isotopic Records 78:1–36
Sachan HK, Sharma R, Sahai A, Gururajan NS (2001) Fluid events and exhumation history of the main central thrust zone Garhwal Himalaya (India). J Asian Earth Sci 19(1–2):207–221
Schotterer U, Fröhlich K, Gäggeler HW, Sandjordj S, Stichler W (1997) Isotope records from Mongolian and alpine ice core as climate indicator. In: Climatic change at high elevation sites. Springer, Dordrecht, pp 287–298
Searle MP, Parrish RR, Hodges KV, Hurford A, Ayres MW, Whitehouse MJ (1997) Shisha Pangmaleucogranite, south Tibetan Himalaya: field relations, geochemistry, age origin and emplacements. J Geol 105(3):295–317
Shivanna K, Tirumalesh K, Noble J, Joseph TB, Gursharan S, Joshi AP, Khati VS (2008) Isotopic techniques to identify recharge areas of springs for rainwater harvesting in the mountainous region of Gaucher areas, Chamoli district, Uttarakhand. India Curr Sci 94:1003
Siegenthaler U, Matter HA (1983) Dependence of $\delta^{18}O$ and δD in precipitation on climate. In: Palaeoclimates and palaeowaters: a collection of environmental isotope studies

Singh SK, Trivedi JR, Pande K, Ramesh R, Krishnaswami S (1998) Chemical and strontium, oxygen, and carbon isotopic compositions of carbonates from the Lesser Himalaya: implications to the strontium isotope composition of the source waters of the Ganga, Ghaghara, and the Indus rivers. Geochim Cosmochim Acta 62(5):743–755

Spencer CJ, Harris RA, Dorais MJ (2012) The metamorphism and exhumation of the Himalayan metamorphic core, eastern Garhwal region, India. Tectonics 31(1):TC1007

Tan H, Zhang W, Chen J, Jiang S, Kong N (2012) Isotope and geochemical study for geothermal assessment of the Xining basin of the northeastern Tibetan Plateau. Geothermics 42:47–55

Tan H, Zhang Y, Zhang W, Kong N, Zhang Q, Huang J (2014) Understanding the circulation of geothermal waters in the Tibetan Plateau using oxygen and hydrogen stable isotopes. Appl Geochem 51:23–32

Tapponnier P, Xu ZQ, Roger F, Meyer B, Arnaud N, Wittlinger G, Yang JS (2001) Geology-oblique stepwise rise and growth of the Tibet plateau. Sci 294:1671–1677

Thakur VC, Rawat BS (1992) Geological map of western Himalaya (explanation). Wadia Institute of Himalayan Geology, Dehra Doon, p 22

Tiwari SK (2014) Isotopic and geochemical studies of geothermal springs of Northwest Himalaya, India: implication for source and degassing of metaphoric CO_2. Doctoral dissertation, Ph. D. thesis, University of Petroleum and Energy Studies, Dehradun, India

Tiwari SK, Bartarya SK, Rai SK, Gupta AK, Asthana AKL (2016a) Isotopic and geochemical studies of groundwater from the Ramganga basin and the middle Ganga Plains: implication for pollution and metal contamination. Environ Earth Sci 75(16):1170

Tiwari SK, Gupta AK, Asthana AKL (2020) Evaluating CO_2 flux and recharge source in geothermal springs, Garhwal Himalaya, India: stable isotope systematics and geochemical proxies. Environ Sci Pollut Res 27(13):14818–14835

Tiwari SK, Kumar A, Gupta AK, Verma A, Bhambri R, Sundriyal S, Yadav J (2018) Hydrochemistry of meltwater draining from Dokriani Glacier during early and late ablation season. West Central Himalaya. Himal Geol 39(1):121–132

Tiwari SK, Rai SK, Bartarya SK, Gupta AK, Negi M (2016b) Stable isotopes ($\delta^{13}C_{DIC}$, δD, $\delta^{18}O$) and geochemical characteristics of geothermal springs of Ladakh and Himachal (India): evidence for CO2 discharge in northwest Himalaya. Geothermics 64:314–330

Tong W, Zhang J (1981) Characteristics of geothermal activities in Xizang Plateau and their controlling influence on plateau's tectonic model. In: Geological and Ecological studies of the Qinghai-Xizang Plateau, pp 841–846

Valdiya KS (1980) Geology of Kumaun lesser Himalaya. Wadia Institute of Himalayan Geology

Valdiya KS (1981) Tectonics of the central sector of the Himalaya. Zagros Hindu Kush Himalaya Geodynamic Evolution 3:87–110

Valdiya KS (1988) Tectonics and evolution of the central sector of the Himalaya Philos Trans Royal Soc A. Math Phys Sci 326(1589):151–175

Valdiya KS (1999) Tectonic and lithological characterization of Himadri (Great Himalaya) between Kali and Yamuna rivers, central Himalaya. Him Geol 20(2):1–17

Veeraswamy K, Abdul Azeez KK, Basava S, Naidu DG, Harinarayana T (2010) Electrical structure across lesser and higher NW. Himalaya India Chinese J Geophys 53(3):576–584

Verma A, Kumar A, Gupta AK, Tiwari SK, Bhambri R, Naithani S (2018) Hydroclimatic significance of stable isotopes in precipitation from glaciers of Garhwal Himalaya, Upper Ganga Basin (UGB). India Hydrol Process 32(12):1874–1893

Witcher JC, King JP, Hawley JW, Kennedy JF, Williams J, Cleary M, Bothern LR (2004) Sources of salinity in the Rio Grande and Mesilla Basin groundwater. New Mexico Water Resources Research Institute Technical Completion Report, 330, 168

Wright WE, Long A, Comrie AC, Leavitt SW, Cavazos T, Eastoe C (2001) Monsoonal moisture sources revealed using temperature, precipitation, and precipitation stable isotope time series. Geophys Res Lett 28(5):787–790

Yin A, Rumelhart PE, Butler R, Cowgill E, Harrison TM, Foster DA, Ingersoll RV, Qing Z, Xian-Qiang Z, Xiao-Feng W, Hanson A (2002) Tectonic history of the Altyn Tagh fault system in northern Tibet inferred from Cenozoic sedimentation. Geol Soc Am Bull 114(10):1257–1295

Yu J, Zhang H, Yu F, Liu D (1984) Oxygen and hydrogen isotopic compositions of meteoric waters in the eastern part of Xizang. Geochem 3(2):93–101

Yurtsever Y, Gat JR (1981) Atmospheric waters. In: Stable isotope hydrology: deuterium and oxygen-18 in the water cycle, pp 103–142

Zhao P, Dor J, Xie EJ, Jin J (2003) Strontium isotope data for thermal waters in selected high-temperature geothermal fields. China Acta Petrologica Sinica 19(3):569–576